Chinese Journal of
POLYMER SCIENCE

RESEARCH ARTICLE

https://doi.org/10.1007/s10118-026-3754-y
Chinese J. Polym. Sci.

Multifunctional Property Enhancement of 2-Acrylamido-2-methyl-1-propanesulfonic Acid/Acrylic Acid Hydrogels with Dual-ionic Liquid Functionalized Carbon Nanotubes

Hui-Wen Jia[a], Xue Lv[a,b*], Yan-Ming Ma[a], Wang Xu[a], and Xiao-Ning Yang[a]

[a] *School of Chemical Engineering, Changchun University of Technology, Changchun 130012, China*
[b] *Changchun Sahala Biochemical Technology Company, Changchun 130012, China*

Electronic Supplementary Information

Abstract Conductive hydrogels with high mechanical strength, good adhesion, and high sensitivity are highly demanded for wearable electronics. A multifunctional hydrogel based on 2-acrylamido-2-methylpropanesulfonic acid (AMPS) and acrylic acid (AA) was synthesized *via* free-radical polymerization. The system incorporates dynamic hydrogen bonds from guanine–cytosine (G–C) base pairs and homogeneously dispersed carbon nanotubes (CNTs) modified using a dual-ionic liquid strategy. Short-chain (C_4) and long-chain (C_{12}) imidazole-based ionic liquids act synergistically to exfoliate and stabilize CNTs, facilitating uniform dispersion and strong interfacial bonding. Owing to the continuous conductive pathways formed by the CNTs, the hydrogel exhibited enhanced electrical conductivity with a gauge factor of 5.61, together with excellent short-term cyclic stability and responsiveness for monitoring dynamic human motions. The combination of covalent cross-linking, reversible hydrogen bonding, and reinforced nanofillers endows the hydrogel with high stretchability, good adhesion (5.5 kPa), and superior fatigue resistance, showing great potential for use in flexible wearable bioelectronics.

Keywords Carbon nanotubes; Ionic liquid; Adhesion; Hydrogels

Citation: Jia, H. W.; Lv, X.; Ma, Y. M.; Xu, W.; Yang, X. N. Multifunctional property enhancement of 2-acrylamido-2-methyl-1-propanesulfonic acid/acrylic acid hydrogels with dual-ionic liquid functionalized carbon nanotubes. *Chinese J. Polym. Sci*. https://doi.org/10.1007/s10118-026-3754-y

INTRODUCTION

In recent years, intelligent sensing technology has developed rapidly,[1–3] promoting breakthroughs in the mechanical adaptability and signal response of flexible electronic devices.[4] Such devices have been able to convert mechanical stimuli such as stretching and bending into electrical signals,[5] and have been widely used in smart healthcare,[6] motion monitoring,[7] bionic robots,[8] and other fields. The mainstream design has used nanocomposites combined with elastic substrates to capture microscopic physiological signals.[9] However, under large deformation or long-term stress, traditional structures have been prone to cracks or failures due to material brittleness and weak interface bonding,[10] and the mechanical mismatch between the conductive layer and the matrix has often led to delamination and has affected durability. Therefore, improving the ductility and structural stability while maintaining high sensitivity has become a key problem in the practical application of flexible electronics.

Hydrogels, as polymer materials with a three-dimensional network structure, have been used in flexible electronics (*e.g.*, wearable sensors) and environmental engineering.[11–18] In recent years, conductive hydrogels have been widely studied due to their inherent softness,[19,20] electrical conductivity,[21] and high stretchability.[22,23] However, traditional conductive hydrogel matrices have been found to have certain limitations,[24] such as the lack of an effective energy dissipation mechanism inside the hydrogel and the uneven dispersion of the conductive material,[25] which have resulted in poor mechanical properties and hindered their wider practical application. To address these problems, numerous strategies have been developed to optimize the mechanical and conductive properties of conductive hydrogels, including the tuning of covalent/physical cross-linking density, blending with rigid polymer substrates, construction of pure dynamic non-covalent bond networks (*e.g.*, hydrogen bonds, metal-ligand coordination,[26,27] hydrophobic interactions) and modification with conventional inorganic nanofillers (*e.g.*, graphene oxide, montmorillonite, silica nanoparticles).[28,29] Carbon nanotubes (CNTs) stand out as an ideal nanofiller for the modification of conductive hydrogels due to their ultra-high aspect ratio, excellent mechanical strength, high electrical conductivity, and good compatibility with hydrophilic polymer networks.[30–32] Compared with other conventional nanofillers, CNTs can form continuous mechanical reinforcement and

* Corresponding author, E-mail: lvxueccut@126.com
Received April 1, 2026; Accepted May 21, 2026; Published online August 28, 2026

electron transport channels in the hydrogel matrix at low addition amounts, realizing the simultaneous improvement of hydrogel mechanical properties and conductivity. To exploit the excellent performance of CNTs, many researchers have carried out in-depth research on functionalization of CNTs and modification of hydrogel composite. Li *et al*.[33] have developed hydrophilic polymer brush-coated CNTs (E-CNTS-PAA) *via* amphiphilic azide block copolymer self-assembly and UV crosslinking, yielding poly(*N*-isopropylacrylamide) (PNIPAM)/E-CNTS-PAA thermal-responsive composite hydrogels. These exhibited remarkable mechanical improvements—tensile strength of 97.7 kPa and elongation of 465%; Khan *et al*.[34] fabricated a conductive hydrogel by incorporating functionalized multiwalled CNTs (F-CNTs) into hydrophobic associative polyacrylamide–lauryl methacrylate (AM/LMA) networks. Using cationic surfactant CDAB, they ensured uniform F-CNT dispersion; carboxylic groups on F-CNTs enabled electrostatic micelle-polymer crosslinking, while CDAB enhanced hydrophobic interactions—resulting in exceptional tensile strain (2016%), toughness (551.56 kJ/m^3), fatigue resistance, and high strain sensitivity (GF=4.69 at 600% strain); Kamaliya *et al*.[35] synthesized Gum ghatti (GG)-cl-poly(acrylic acid)(AA)/o-multiwalled carbon nanotubes (MWCNTs) hydrogels *via* radical copolymerization, resolving CNT dispersion *via* oxidative MWCNT modification and boosting mechanics through GG–AA crosslinking and *o*-MWCNT reinforcement; Fu *et al*.[36] constructed MWCNTs/ZIF-8/agarose–sodium alginate (MZASA) hydrogel beads by *in situ* ZIF-8 binding onto MWCNTs and dual-network integration, followed by Ca^{2+} crosslinking, which improved mechanical robustness, while MWCNTs/zeolitic imidazolate frameworks-8 (ZIF-8) increased the surface area and dye adsorption capacity. Collectively, effective CNT dispersion emerges as a critical factor for optimizing the conductivity, mechanics, stimuli-responsiveness, and multifunctionality of advanced hydrogels.

At the same time, hydrogels have poor adhesion to the skin or other substrates, making them susceptible to detachment, affecting the stability of signal acquisition and long-term use. To solve this problem, dopamine-o-phenylenediamine has usually been introduced. Wang *et al*.[37] developed a multifunctional supramolecular hydrogel (PXNT) by integrating poloxamer 407 (PX), ROS-scavenging/anti-inflammatory tannin–cyclodextrin nanoparticles (TPCDNP), and adhesion-promoting tannic acid (TA).Through systematic *in vitro* screening and *in vivo* validation, PXNT demonstrated synergistic anti-inflammatory, antioxidant, antifibrotic, bioadhesive, self-healing, and temperature-responsive properties. Critically, it significantly suppressed dural fibrosis and post-laminectomy adhesions in rat and rabbit models—highlighting its translational potential for spinal surgery applications.

Nucleobases are abundant and have numerous interaction sites, such as hydrogen bonding, π-π stacking, and van der Waals forces, which have allowed them to interact with and functionalize other molecules.[38] Shi *et al*.[39] developed a nucleobase-functionalized poly-L-glutamic acid derivative exhibiting 0.5 MPa adhesion, demonstrating the effectiveness of nucleobases in enhancing viscosity.

In this work, we have innovatively employed a dual ionic liquid (C_4/C_{12})-assisted strategy to disperse carbon nanotubes (CNTs), using short-chain ([C_4mim]Cl) and long-chain ([C_{12}mim]Cl) imidazolium-based ionic liquids to achieve stepwise stripping and stabilization of CNTs in aqueous media, and the synergistic effects of π-π stacking, electrostatic interaction, and steric hindrance have enabled the formation of homogeneously dispersed carbon nanotube networks. At the same time, hydrogels have been constructed based on the copolymerization reaction of AMPS and AA, and we have used the nucleobases as dynamic hydrogen bonding units to enhance energy dissipation. The resulting covalently crosslinked P(AMPS-*co*-AA) chains and physically crosslinked Nucleobases guanine-cytosine (G-C) interaction have achieved a significant mechanical enhancement through a double network structure. The composite hydrogels have exhibited excellent properties, including ultra-high stretchability (2320%), excellent toughness, fast response time (300 ms), high strain sensitivity (GF=5.61), and good adhesion (5.5 kPa). The combined properties have enabled the hydrogel to be a viable candidate for advanced wearable strain sensors and flexible electronic devices.

METHODS

Reagents

2-Acrylamide-2-methylpropionic acid (AMPS), acrylic acid (AA), carbon nanotubes (C), *N*,*N*-methylenebis(acrylamide) (MBA), guanine (G), cytosine (C), [C_4mim]Cl, and [C_{12}mim]Cl were purchased from Shanghai Aladdin Reagent Co., Ltd., and potassium persulfate (KPS) was provided by Tianjin Fuchen Chemical Reagent Co., Ltd. All reagents were analytical-grade and did not require further purification prior to use.

Preparation of ILs@C

Ionic liquids (ILs) with an alkyl chain length of 4 (0.025g) were dissolved in 100 mL of deionized water to prepare a pre-dispersible solution, carbon nanotubes (C) were added to the solution, sonicated for 30 min, and the C was initially dispersed. Centrifuged the mixed solution (10000 r/min for 8 min) and washed several times. The centrifugally separated product was freeze-dried to obtain a black powder. Then, dissolved it in 100 mL of deionized water, added ionic liquids (ILs) with an alkyl chain length of 12 (0.075 g), and finally dispersed C, using the same steps as above, and finally obtained ILs@C powder. The detailed process of the modification of carbon nanotubes by ILs has been shown in Fig. S1 (in the electronic supplementary information, ESI).

Synthesis of A-PS-G-C-ILs@C Hydrogels

Dissolved 0.6 g of guanine (G) and 0.6 g of cytosine (C) in 20 g of deionized water and stirred for 2 h at room temperature (25 °C). Then added 6 g of acrylic acid (AA), 2 g of 2-acrylamide-2-methylpropanesulfonic acid (AMPS), 0.2 g of ILs@C and 0.01 g of *N*,*N*-methylene bis(acrylamide) (MBA) to the mixed solution and mixed well with magnetic stirring for 4 h. Finally, 0.1 g of potassium persulfate (KPS) was added, stirred, poured into the mold and placed in a 60 °C oven for 6 h to polymerize to prepare the hydrogel.

Characterization

Fourier transform infrared spectroscopy (FTIR) test

Fourier transform infrared spectroscopy was used to analyze the

changes in the carbon tube functional groups before and after modification. Carbon tube samples of different modifications were mixed with potassium chloride at a mass ratio with 1:100, ground thoroughly, pressed into transparent sheets, and the vibration absorption of the samples in the 4000–500 cm^{-1} scanning area was recorded.

Scanning electron microscope (SEM) test

The geomorphological characteristics of the hydrogel were observed using scanning electron microscopy (SEM, ZEISS, Gemini). The hydrogel sample was immersed in liquid nitrogen and fractured with forceps to expose the cross-section. After gold plating, the fractured surfaces were imaged using a scanning electron microscope.

Mechanical properties test

The mechanical properties of hydrogels were evaluated using a universal testing machine (Shimadzu, AGS-X, 100 N, Japan). The hydrogel sample was cut into dumbbell shapes with dimensions of 20 mm long, 2 mm wide and 4 mm thick, and then the cut sample was fixed between the two fixtures of the testing machine. Used a vernier caliper to measure the initial length of each sample. The sample was then tested at a tensile speed of 100 mm/min. In order to control the experimental error, three sets of samples were prepared in parallel for each formulation and tested independently.

Fatigue resistance and self-healing performance tests

Cyclic tensile and compression tests were performed using a universal testing machine (Shimadzu, AGS-X, 100 N, Japan). For compression testing, a cylindrical hydrogel sample with a diameter of 10 mm was prepared. The sample was held in the middle of the two fixtures and the initial length of the fixture was measured with a vernier caliper. Compression was performed at a constant rate (20 mm/min) during loading. To ensure consistency and data accuracy, three hydrogel samples were prepared and tested.

Conductivity test

The hydrogel was cut into rectangular samples, placed on a four-probe mold made of Teflon and its resistance R was measured at room temperature using an electrochemical workstation in the frequency range of 0.1–100 kHz. The conductivity was calculated by a formula, and each set of samples was repeated five times and the value was averaged.

The formula for calculating conductivity is as follows:

$$\sigma = \frac{L}{RS} \tag{1}$$

where σ is the conductivity (mS/cm), R is the resistance of hydrogel, L is the distance between the electrodes(cm), and S is the effective area of the hydrogel (cm^2).

Adhesion performance test

The adhesion properties of hydrogels on different substrates were evaluated by lap experiments. The tested substrates included polyvinyl chloride, polyethylene terephthalate, glass, and pigskin. The hydrogel was cut into cubes of (length, width, and height) 2 cm × 2 cm × 0.1 cm. The samples were placed between two pieces of the same substrate, manually pressed for several minutes to ensure good contact, and a lap shear test was performed using a universal testing machine (model Shimadzu, AGS-X, 100 N, Japan) with a tensile rate of 2 mm/min, and each sample was measured under these conditions to assess its bond strength.

Sensing performance and human motion monitoring

The sensing properties of composite hydrogels were investigated using a combination of a universal testing machine (Shimadzu, AGS-X, 100 N, Japan) and an electrochemical workstation (Princeton Applied Research Model 2273). In the testing process, the universal test was set up to apply axial tension to the columnar hydrogel specimen at a constant rate (100 mm/min), and the material resistance change curve was collected synchronously at the workstation to construct the strain-resistance correspondence model. The hydrogel was fixed on the sensitive tissue of the human body, the two ends of the hydrogel were connected with the electrochemical workstation, and the dynamic change of resistance (R) with human movement was recorded, and a human motion detection test was performed.

The formula for calculating relative resistance is as follows:

$$\Delta R/R_0\ (\%) = (R - R_0)/R_0 \times 100 \tag{2}$$

where R is the real-time resistance, and R_0 is the initial resistance.

The formula for calculating the strain coefficient (GF) is as follows:

$$\mathrm{GF} = ((R - R_0)/R_0)/\varepsilon \tag{3}$$

where R, R_0, and ε represent real-time resistance, initial resistance, and tensile strain, respectively.

DISCUSSION

Synthesis Mechanism of A-PS-G-C-ILs@C Hydrogels

P(AMPS-*co*-AA)-G_n-C_n-ILs@C hydrogels (A-PS-G_n-C_n-ILs@C) with multiple network structures were successfully prepared by radical polymerization (n indicated different contents). Fig. 1 shows a schematic diagram of the preparation process of A-PS-G_n-C_n-ILs@C hydrogel. Under the activation of a potassium persulfate (KPS) initiator, 2-acrylamide-2-methylpropionic acid (AMPS) and acrylic acid (AA) monomers copolymerized, and potassium persulfate decomposed to produce sulfate during thermal activation, which triggered vinyl polymerization and promoted the continuous growth of hydrophilic polymer chains. The covalent crosslinker *N*,*N*'-methylene biacrylamide (MBA) constructed permanent junctions between polymer chains through a covalent crosslinking strategy, forming a stable three-dimensional hydrogel matrix.

To improve the adhesion and mechanical properties, guanine-cytosine (G-C) complementary base pairs were introduced into the hydrogel network in 3D networks. G-C based pairs form dynamically reversible hydrogen bonds that served as physical crosslinking points. These physical crosslinking nodes with dynamic reversible characteristics significantly improved the energy dissipation efficiency of the system through the energy dissipation mechanism of dynamic fracture and reconstruction when the material was subjected to mechanical load.

To impart electrical conductivity to the hydrogel, carbon nanotubes (C) were stripped using a dualionic liquid. Firstly, a short-chain ionic liquid (C_4) was used to predisperse the carbon nanotubes, and its small molecule size advantage was used to quickly penetrate into the carbon nanotube bundle gap, and the van der Waals force between the nanotubes was weakened by the cation-π stacking effect and charged inter-

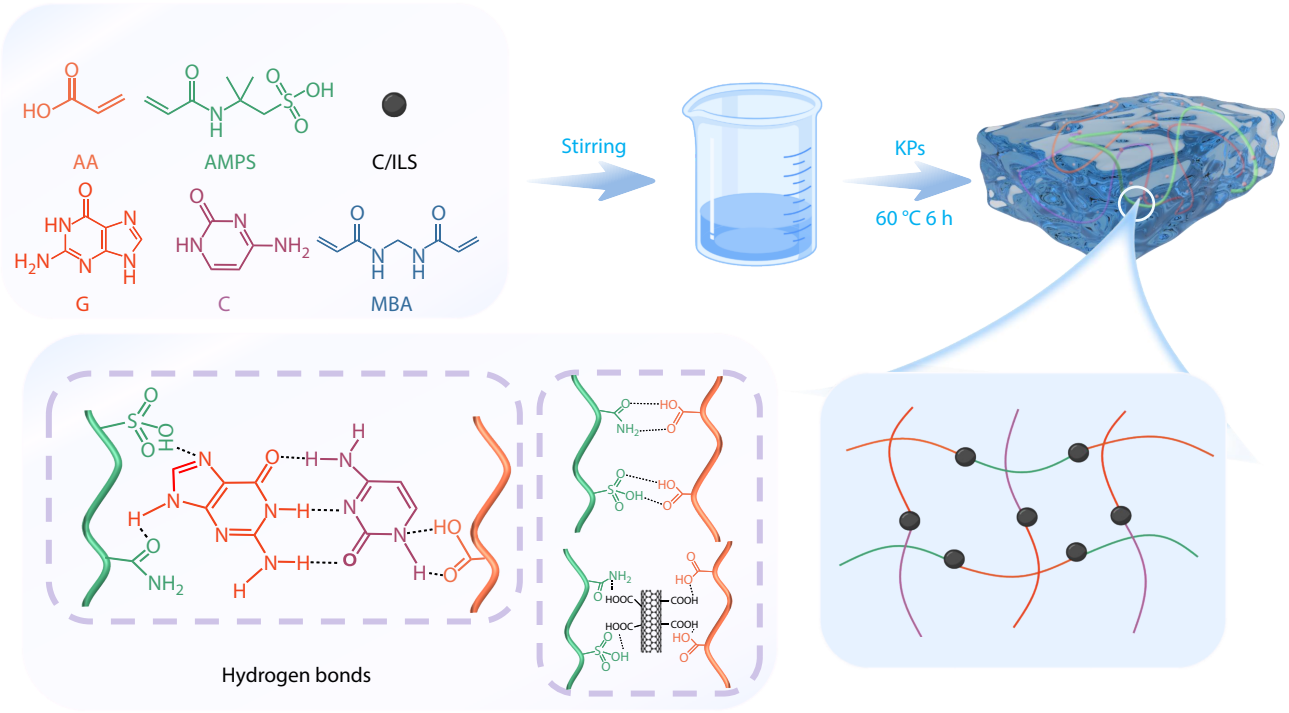

Fig. 1 Preparation and mechanism of A-PS-G-C-ILs@C hydrogels.

action, and then the long-chain ionic liquid (C_{12}) was used for secondary stripping, and the surface of the CNTS was wrapped through the steric hindrance effect of the long alkyl chain, forming a stable spatial barrier to prevent reagglomeration. This step-by-step processing strategy allowed the conductive carbon nanotubes to disperse evenly throughout the hydrogel matrix, forming a continuous conductive path.

There were multiple interactions in the composite hydrogels: the AMPS-AA copolymer chains formed a rigid framework through strong covalent bonds, the dynamic hydrogen bond network formed by G-C base pairs provided energy dissipation pathways, and the uniformly dispersed carbon nanotubes constructed continuous electron transport channels. This multi-scale synergistic mechanism allowed the material to maintain its structural integrity while providing excellent conductivity and mechanical response properties.

Modification of CNTs

To solve the problem that carbon nanotubes were difficult to dissolve in polar water, we used ionic liquids to enhance their dispersibility. By systematically comparing the dispersion efficiency of ionic liquids with different chain lengths (single ionic liquid (alkyl chain length 4 and alkyl chain length 12) and composite system C_4/C_{12}), we found that the bifunctional ionic liquid system showed a unique synergistic effect. Fig. S2(b) (in ESI) shows the FTIR spectra of ILs@C, in which there are obvious C—H elastic vibration absorption bands at 2920 and 2850 cm^{-1}, and the peak strength increased with the change of alkyl chain length and intercalation combination, indicating that the long-chain alkyl groups in ILs were effectively introduced into the C structure. At the same time, the wide peak of the sample was enhanced around 3400 cm^{-1}, indicating that imidazole cations formed hydrogen bonds with the C surface, which further supported the existence of interfacial interactions. In addition, the new absorption peaks in the 1000–1500 cm^{-1} region can be attributed to the characteristic vibrations of functional groups such as C—N and C—O—C, further confirming the existence of ionic liquid components on the C surface or channel. In the low-wave number region, the C_{12} and C_{4+12} intercalations exhibited enhanced CH_2 swaying vibrations, especially C_{12} in the intercalation samples, indicating that the long chain structure was more fully covered by the C surface. The short-chain ionic liquid (C_4) was first inserted into the carbon tube bundle gap and the van der Waals force was weakened through π-cation interaction. The subsequent introduction of a long-chain ionic liquid (C_{12}) significantly inhibited the reaggregation trend of nanotubes by tangling alkyl chains.

Structure and Morphology of A-PS-G-C-ILs@C Hydrogels

In order to delve into the microscopic morphology of hydrogels, we pretreated them by freeze-drying method and observed them by scanning electron microscopy. As shown in (Fig. 2), all hydrogels exhibited a typical three-dimensional porous network structure. The pore structures of A-PS hydrogels (Fig. 2a) were irregular and the pore size distribution was wide. With the introduction of G-C and ILs@C (Figs. 2b and 2c), the pore wall of the hydrogel thickened significantly, the pore arrangement tended to be regular, showed a uniform honeycomb structure, and the ILs@C was uniformly embedded in the A-PS polymer network, and no obvious agglomeration phenomenon was observed. This was due to the hydrogen bonding between guanine, cytosine and the internal structure of the hydrogel, which made hydrogel structure more uniform. On the one hand, this uniform and stable composite network structure strengthens the polymer skeleton as a physical cross-linking point, thereby improving the mechanical properties of the hydrogel. On the other hand, the ordered pore structure also provided an effec-

tive path for the continuous transport of electrons, which was conducive to enhancing conductivity.

Mechanical Property of A-PS-G_n-C_n-ILs@C Hydrogels

We used radical polymerization to prepare A-PS-G_n-C_n-ILs@C composite hydrogels. First, we explored the optimal content ratio of AA-AMPs (Fig. 3a). We investigated the effects of different G-C contents on the mechanical properties of hydrogels by adding different amounts of G-C to AA-AMPs to explore the optimal G-C content. The hydrogels with different G-C contents were analyzed by tensile test, and the gradient changed of G-C molar ratio in the range of 0.2:0.2 to 0.8:0.8, namely A-PS-$G_{0.2}$-$C_{0.2}$-ILs@C, A-PS-$G_{0.4}$-$C_{0.4}$-ILs@C, A-PS-$G_{0.6}$-$C_{0.6}$-ILs@C, A-PS-$G_{0.8}$-$C_{0.8}$-ILs@C, evaluate its elastic modulus.

With the gradual increasing of G-C content (Fig. 3b), the mechanical properties were significantly improved (26, 32, 36 and 33 kPa) and the corresponding strain also was 1414%, 1654%, 2320% and 611%. Fig. 3(c) shows the corresponding toughness. When the G-C ratio was 0.6:0.6, the fracture toughness of the hydrogel reached maximum value, showed the optimal performance. This enhancement effect was mainly attributed to the reversible dynamic hydrogen bonds formed between the G-C bases, which effectively dissipated energy. Nevertheless when the G-C content exceeded 0.6:0.6, excessive dynamic hydrogen bonds led to over-crosslinking of the hydrogel network. The rigid physical crosslinking points restrict the sliding and extension of polymer chains, reducing the chain ductility and causing a sharp decrease in fracture strain. In addition, CNTs were embedded in the hydrogel three-dimensional network through physical entanglement, and crack propagation was inhibited with the help of mechanical interlocking and stress transfer mechanisms. This synergy constructs an efficient energy dissipation path, significantly improving the overall mechanical performance of the material. As shown in Fig. 3(j), it is in the tensing process (Fig. 3j-ii), load-bearing (Fig. 3j-iii), torsion (Fig. 3j-iv), bending (Fig. 3j-v) and even knotting (Fig. 3j-vi), which fully verifies its excellent mechanical strength and toughness.

Hydrogel Fatigue Resistance and Self-healing Properties Test

As a soft material, fatigue resistance directly determined its actual service life. In order to evaluate the durability of the A-PS-$G_{0.6}$-$C_{0.6}$-ILs@C hydrogel after optimizing the ratio, the stress-strain curve was shown in Fig. 3(d). At 100% strain, the first load-unload cycle showed a significant lag loop and the 2nd to 10th cyclic curves gradually approached each other, indicating that the internal structure of the material tended to be stable and

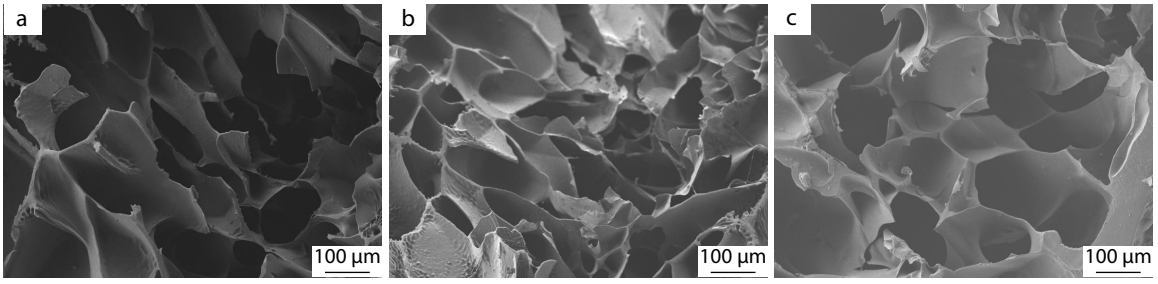

Fig. 2 SEM diagrams of (a) A-PS hydrogels, (b) A-PS-G–C hydrogels and (c) A-PS-$G_{0.6}$–$C_{0.6}$ -ILs@C hydrogels.

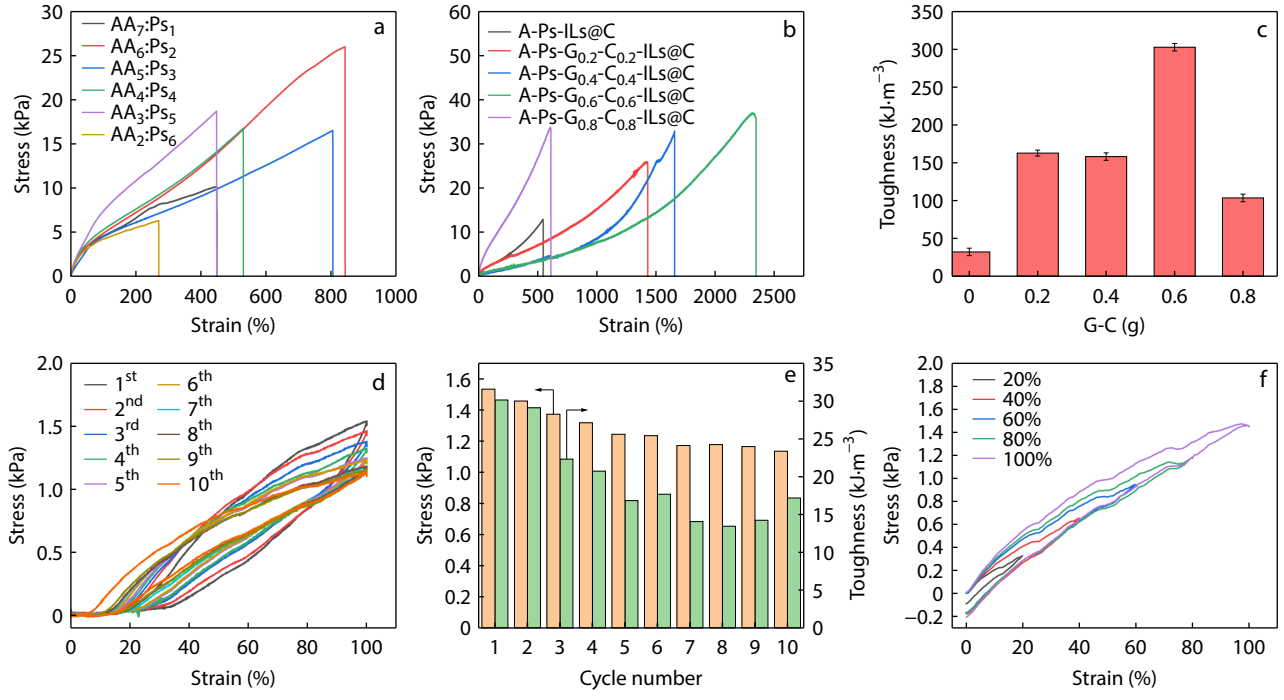

https://doi.org/10.1007/s10118-026-3754-y

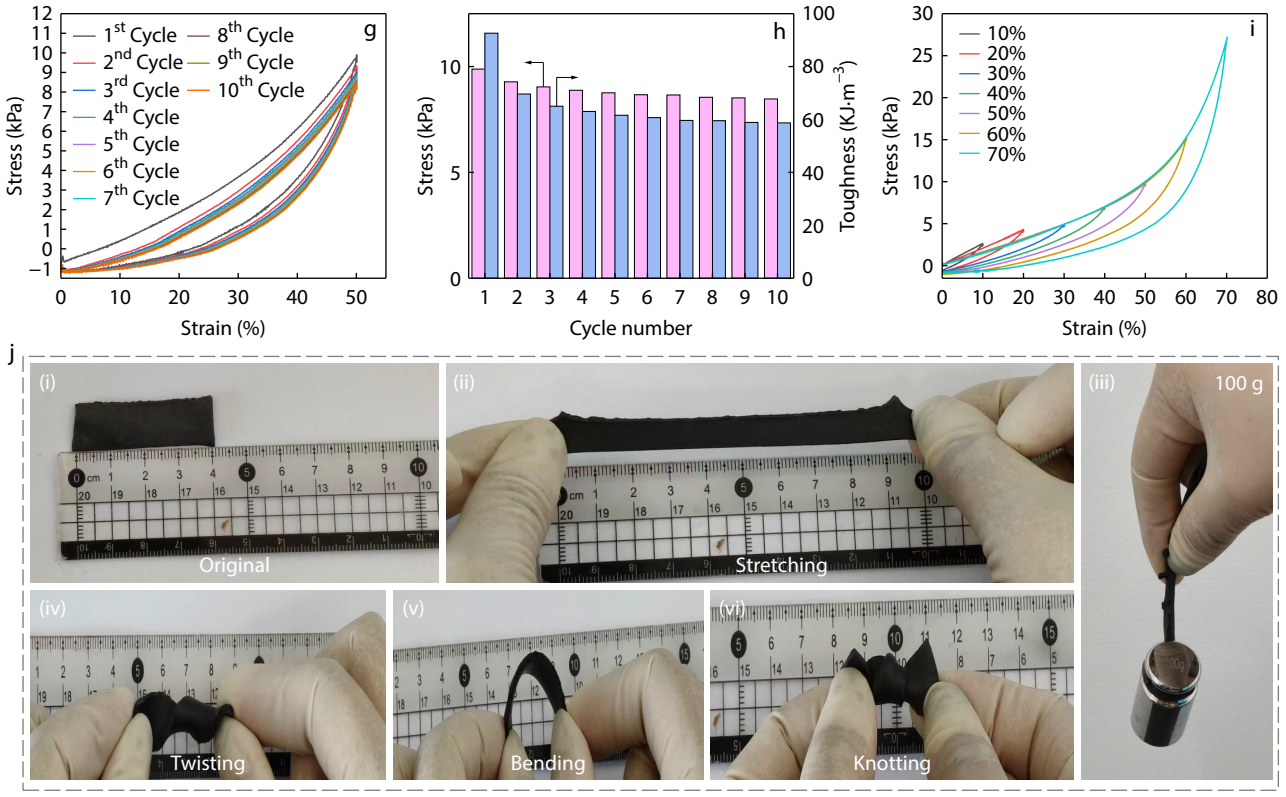

Fig. 3 Mechanical properties of hydrogels. (a) A-PS hydrogel tensile stress-strain curve; (b) A-PS-G_n-C_n-ILs@C hydrogel stress-strain curves; (c) Corresponding resilience; (d) A-PS-$G_{0.6}$–$C_{0.6}$-ILs@C tensile cycle curve of hydrogel at 100% strain; (e) Corresponding toughness and stress; (f) Cyclic tensile stress-strain curves of A-PS-$G_{0.6}$–$C_{0.6}$-ILs@C hydrogel under different strains; (g) Stress-strain curves of A-PS-$G_{0.6}$–$C_{0.6}$-ILs@C hydrogel compression; (h) Corresponding toughness and stress; (i) Cyclic compressive stress-strain curves of A-PS-$G_{0.6}$–$C_{0.6}$-ILs@C hydrogels under different strains; (j) Mechanical properties of A-PS-$G_{0.6}$–$C_{0.6}$-ILs@C hydrogels: (i) original, (ii) stretching, (iii) load-bearing, (iv) twisting, (v) bending, (vi) knotting.

uniform after the initial deformation. As a result, the subsequent nine load-unload curves almost overlapped, and the dissipated energy remained at 57% after ten cycles. Fig. 3(e) shows the corresponding toughness and stress values. Fig. 3(f) shows the stress-strain curve of the A-PS-$G_{0.6}$-$C_{0.6}$-ILs@C hydrogel under continuous tensile cycles under different strains. When the strain increased from 20% to 100%, the lag ring widened significantly as the strain increased from 20% to 100%, reflecting the stronger energy dissipation capacity under large deformations. This excellent short-term cyclic stability stemmed from the synergistic mechanism between dynamic cross-linking and covalent networks. During cyclic loading, the dynamic reversible hydrogen bonds between G-C base pairs were preferentially broken to dissipate energy, while the covalent backbone ensured that the overall structure was not destroyed. After uninstallation, dynamic keys quickly self-heal, and restoring microstructural integrity. In addition, the overall structure was not destroyed. When uninstalled, the dynamic bonds quickly self-heal, restoring microstructural integrity. At the same time, the introduced carbon nanotubes effectively inhibited crack propagation through physical entanglement, further extending the fatigue life. We further examined its compressive strength and recovered properties. The cyclic compression test (Fig. 3g) showed that the compression modulus decreased after 10 compression cycles at 50% strain, and the hysteresis ring area gradually decreased with the increase of the number of cycles, indicating that the internal energy dissipation mechanism of the material remained stable under long-term loading. Fig. 3(h) shows corresponding toughness and stress. Fig. 3(i) shows the compressive cyclic stress-strain curve under different strains, and when the strain was increased from 20% to 100%, the hydrogel showed a significant hysteresis loop. The large hysteresis loop and high peak stress in the first cycle are attributed to the Mullins effect: G-C dynamic hydrogen bonds are broken to dissipate energy during the first stretching. In subsequent cycles, hydrogen bonds rapidly reform, leading to stable cyclic performance, and finally give the hydrogel good durability and compliance.

The A-PS-$G_{0.6}$-$C_{0.6}$-ILs@C hydrogel was connected to a simple circuit consisting of a light-emitting diode and a power supply in series to evaluate its strain response performance (Fig. 4). After closing the switch, the LED light was illuminated, indicating that the hydrogel could conduct electricity. During the stretching process, the brightness of the LED lamp gradually decreased as the degree of deformation increased, indicating that the material was highly sensitive to mechanical strain. After releasing the stretch, the LED would return to its original brightness; When the hydrogel was cut off, the circuit was interrupted and the LED went out immediately; Once the fracture surface was re-contacted, the light was immedi-

https://doi.org/10.1007/s10118-026-3754-y

ately restored, proving that the material had excellent self-healing function. The experimental results fully verified that the hydrogel had good strain sensing ability and self-healing characteristics, and showed its application potential in the field of flexible electronics.

Conductivity Test

As we all know, hydrogels needed to have good electrical conductivity in implantable electronic products. The conductivity of A-PS-$G_{0.6}$-$C_{0.6}$-ILs@C hydrogels were mainly due to the electron conduction of the CNTs. As shown in Fig. S3 (in ESI), the conductivity of the hydrogel was 3.4 mS/cm without the addition of CNTs. After that, the conductivity increased to 8.75 mS/cm with the increase of CNTs.

Adhesion Properties of Hydrogels

Fig.5(a) shows that A-PS-$G_{0.6}$-$C_{0.6}$-ILs@C hydrogels exhibited excellent adhesion to a variety of inorganic and organic substrates, including iron, glass, resin, rubber, and biological tissues such as pig skin, pig intestines, and pig liver. To further quantify its adhesion capacity, lap shear experiments were performed, and the schematic illustration of the lap shear test was displayed in Fig. 5(b). As shown in Figs. 5(c) and 5(d), the adhesion strength of the hydrogel to PVC, pig skin, glass and PET was 2.94, 3.13, 4.4 and 5.55 kPa, respectively. Among them, the high adhesion of hydrogel to pig skin was mainly due to the chemical interaction between the hydroxyl group on the surface of pig skin and the functional group on the PAA hydrogel chain. This tissue adhesion property made it possible for A-PS-$G_{0.6}$-$C_{0.6}$-ILs@C hydrogels to stably adhere to biological tissue surfaces, showed great potential as flexible sensor materials. Further analysis revealed (Fig. 5e) that its good adhesion was due to the abundance of carboxyl, sulfonic and amino groups on the PAA chain, which could effectively bind to different interfaces through hydrogen bonding and electrostatic action, resulting in broad and good

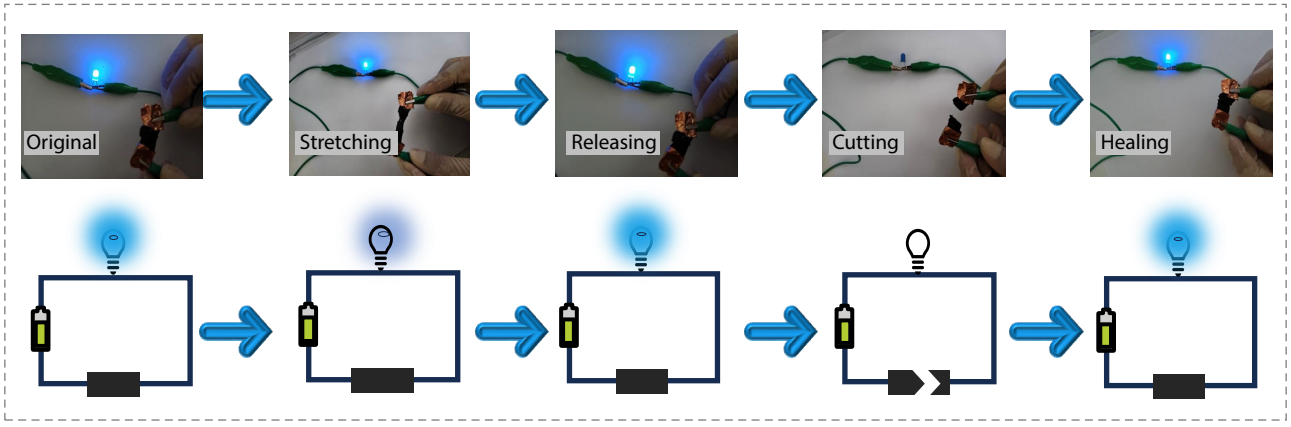

Fig. 4 Hydrogel self-healing properties and LED brightness changes after stretching.

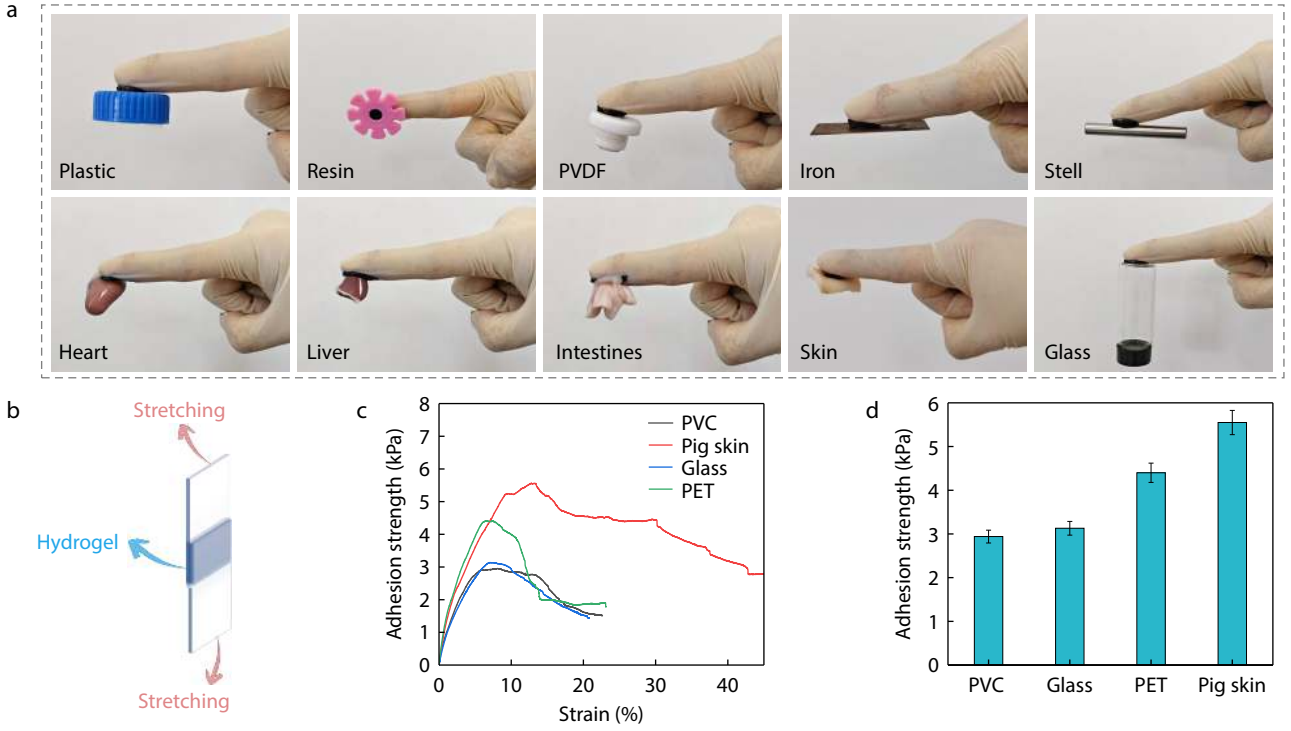

https://doi.org/10.1007/s10118-026-3754-y

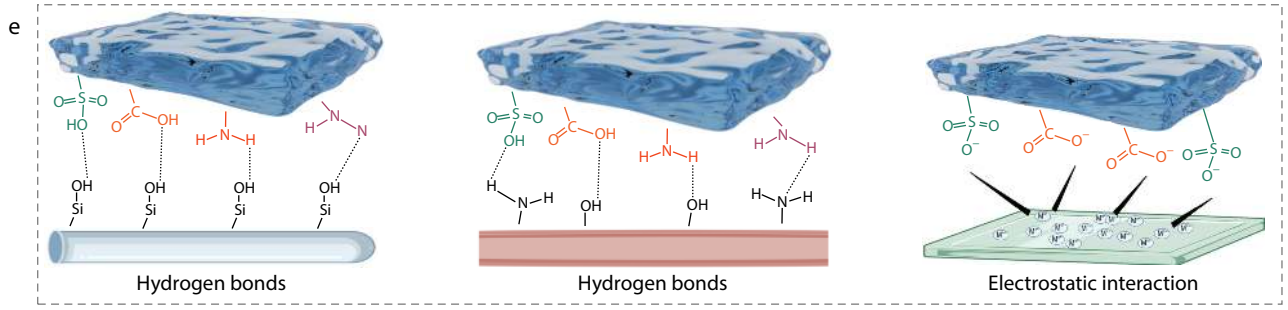

Fig. 5 Adhesion properties of hydrogels. (a) Adhesion properties of A-PS-$G_{0.6}$–$C_{0.6}$-ILs@C hydrogels on different substrate surfaces; (b) Schematic illustration of lap shear test; (c) Adhesion curves of A-PS-$G_{0.6}$–$C_{0.6}$-ILs@C hydrogels on different substrates; (d) Maximum adhesion of A-PS-$G_{0.6}$–$C_{0.6}$-ILs@C hydrogels on different substrates; (e) Schematic diagram of the adhesion mechanism of A-PS-$G_{0.6}$–$C_{0.6}$-ILs@ hydrogels Note: the hydrogel is shown in light color for simplified schematic representation; the actual composite hydrogel with CNTs is black/dark gray.

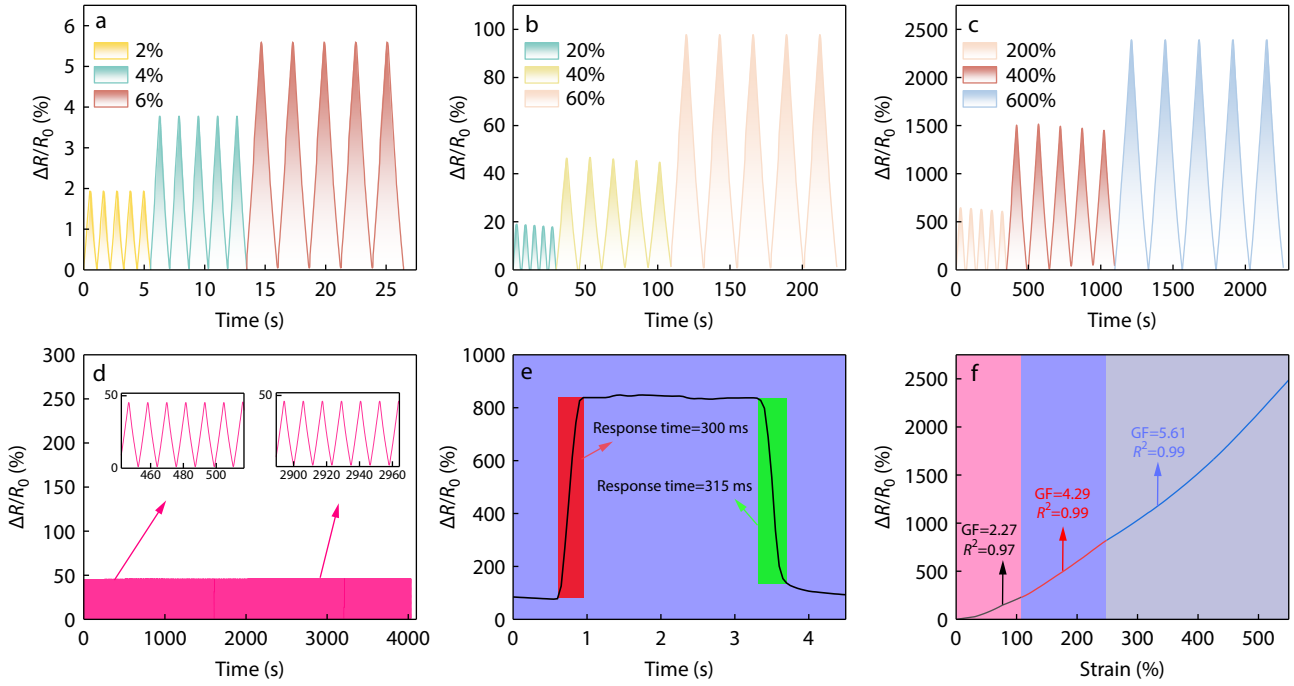

Fig. 6 Conductivity and sensing performance of hydrogels. (a) Changes in relative resistance of hydrogel sensors under small strains (2%, 4%, 6%); (b) Relative resistance changes of hydrogel sensors under moderate strain (20%, 40%, 60%); (c) Changes in the relative resistance of hydrogel sensors under large strains (200%, 400%, 600%); (d) Cyclic stability test at 0% to 40% strain; (e) A-PS-$G_{0.6}$–$C_{0.6}$-ILs@C response and recovery time of composite hydrogels; (f) Change in relative resistance and GF value under continuous tensile strain (0%–600%).

adhesion.

Sensing Performance and Human Motion Monitoring

We investigated the sensing properties of composite hydrogels using a dynamic mechanical-electrochemical coupling system to monitor the relative resistance changes ($\Delta R/R_0$) during tensile and compression deformation in real time. The experimental results showed that the hydrogel showed a continuous increase in resistance response with the increase of strain in three typical deformation stages (Figs. 6a–6c): small strain (2%, 4%, 6%), medium strain (20%, 40%, 60%), and large strain (200%, 400%, 600%). This change stemmed from the decrease of cross-sectional area and the decrease of conductive path density due to the length extension during the deformation of the material, resulting in an increase in resistance and a decrease in current. To assess its long-term stability, we examined stability at 0% to 40% strain (Fig. 6d) and found that its relative resistance value remained stable without significant fluctuations. This excellent signal stability was due to the energy dissipation mechanism of the three-dimensional network structure of the material, indicating that the sample was very stable during cycling, further demonstrating the excellent signal repeatability and structural durability of the hydrogel under repeated deformation. The composite hydrogel also exhibited rapid electromechanical responsiveness during fast loading and unloading. The response time for the tensile and recovery processes (Fig. 6e) were 300 and 315 ms, respectively. At the same time, the relative resistance change curve was shown in Fig. 6(f). The gauge factor (GF) was calculated to be 2.27, 4.29 and 5.61 within the strain ranges of 0%–100%, 100%–250% and 250%–600%.The sensitivity of the hydrogel was due to the synergistic effect of its porous structure and carbon nanotube network: the pores were enlarged during stretching, and the CNTs spacing was increased,

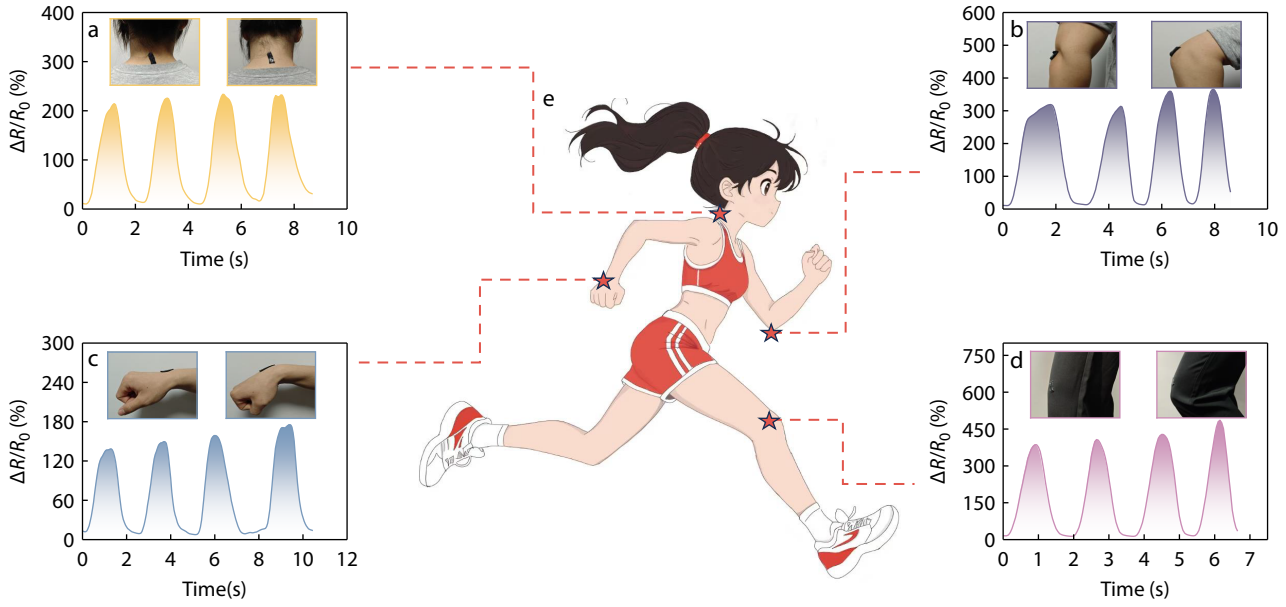

Fig. 7 Hydrogel sensor for monitoring electrical signals. Human joint sensing diagram: monitoring of the (a) neck, (b) elbow, (c) wrist, and (d) knee joints, (e) schematic illustration of human body showing strain sensors attached to the corresponding joints.

significantly changing the conductive pathway and thus amplifying the resistance change. The A-PS-$G_{0.6}$–$C_{0.6}$-ILs@C hydrogel sensor exhibited relatively high GF levels, demonstrating its immense potential in manufacturing strain sensors.

As a wearable sensor, the hydrogel was used to detect different body movement states of various joints and parts of the human body, exhibiting stable strain response and significant electrical stability. From Fig. 7, we could clearly see that when it was attached to the knee joint, neck, elbow and wrist, the sensor can immediately generate the corresponding electrical signal as the material is deformed by limb movement. Through in-depth analysis of the relative resistance curve feedback from the gel sensor, the motion of different human joints can be distinguished. This result further confirmed that the sensor not only had excellent electrical stability, but also had good sensitivity.

CONCLUSIONS

This study presented a robust and versatile conductive hydrogel engineered by integrating a P(AMPS/AA) copolymer network with dynamic G–C hydrogen bonds and a dual-ionic-liquid-modified CNTs dispersion strategy. The synergy of covalent cross-linking, reversible physical interactions, and a uniform CNTs network endowed the hydrogel with remarkable mechanical properties, excellent short-term cyclic stability and good fatigue resistance. Furthermore, the CNTs network ensured stable and sensitive electrical conductivity. With its self-healing capability and good adhesion, this hydrogel meets the multifaceted requirements of next-generation wearable sensors, offering a rational design strategy for advanced flexible electronics and human-machine interfaces.

Conflict of Interests

The authors declare no interest conflict.

Electronic Supplementary Information

Electronic supplementary information (ESI) is available free of charge in the online version of this article at http://doi.org/10.1007/s10118-026-3754-y.

Data Availability Statement

The data supporting the findings of this study are available from the corresponding author upon reasonable request.

ACKNOWLEDGMENTS

This work was financially supported by the Department of Science and Technology of Jilin Province (No. YDZJ202601ZYTS089).

REFERENCES

1 He, Y.; Liang, Y.; Gao, W.; Duan, X.; Guan, Y. High-fidelity distributed Brillouin sensing with optical mechanisms fusion and data transfer. *Eng. Sci.* **2025**, *38*, 1922.
2 Wang, P.; Hu, M.; Wang, H.; Chen, Z.; Feng, Y.; Wang, J.; Ling, W.; Huang, Y. The evolution of flexible electronics: From nature, beyond nature, and to nature. *Adv. Sci.* **2020**, *7*, 2001116.
3 Zeng, Y.; Tang, L.; Xiao, S.; Dong, Z.; Li, X.; Wang, T.; Liu, X.; Ma, Y.; Chu, F. A multi-sensor information fusion fault diagnosis method for hydropower turbine bearings based on multi-scale spatiotemporal graph neural networks. *Eng. Sci.* **2025**, *38*, 1882.
4 Li, S.; Bi, Y.; Liu, J.; Fu, G.; Chai, H.; Sun, C.; Feng, W. High-sensitivity piezoresistive biomass-derived carbon aerogel/polydimethylsiloxane composite with extreme temperature adaptability. *Energy Environ. Mater.* **2026**, *9*, e70079.
5 Xiang, X.; He, Q.; Xia, S.; Deng, Z.; Zhang, H.; Li, H. Study of capacitance type flexible electronic devices based on polyacrylamide and reduced graphene oxide composite hydrogel. *Eur. Polym. J.* **2022**, *171*, 111200.

Graphical Abstract

Multifunctional Property Enhancement of 2-Acrylamido-2-methyl-1-propanesulfonic Acid/Acrylic Acid Hydrogels with Dual-ionic Liquid Functionalized Carbon Nanotubes

Hui-Wen Jia, Xue Lv, Yan-Ming Ma, Wang Xu, and Xiao-Ning Yang

Changchun University of Technology; Changchun Sahala Biochemical Technology Company

A high-stretch, adhesive and self-healing conductive hydrogel was constructed *via* guanine-cytosine (G-C) hydrogen bonds and ionic liquid functionalized carbon nanotubes (CNTs) for wearable motion sensing.

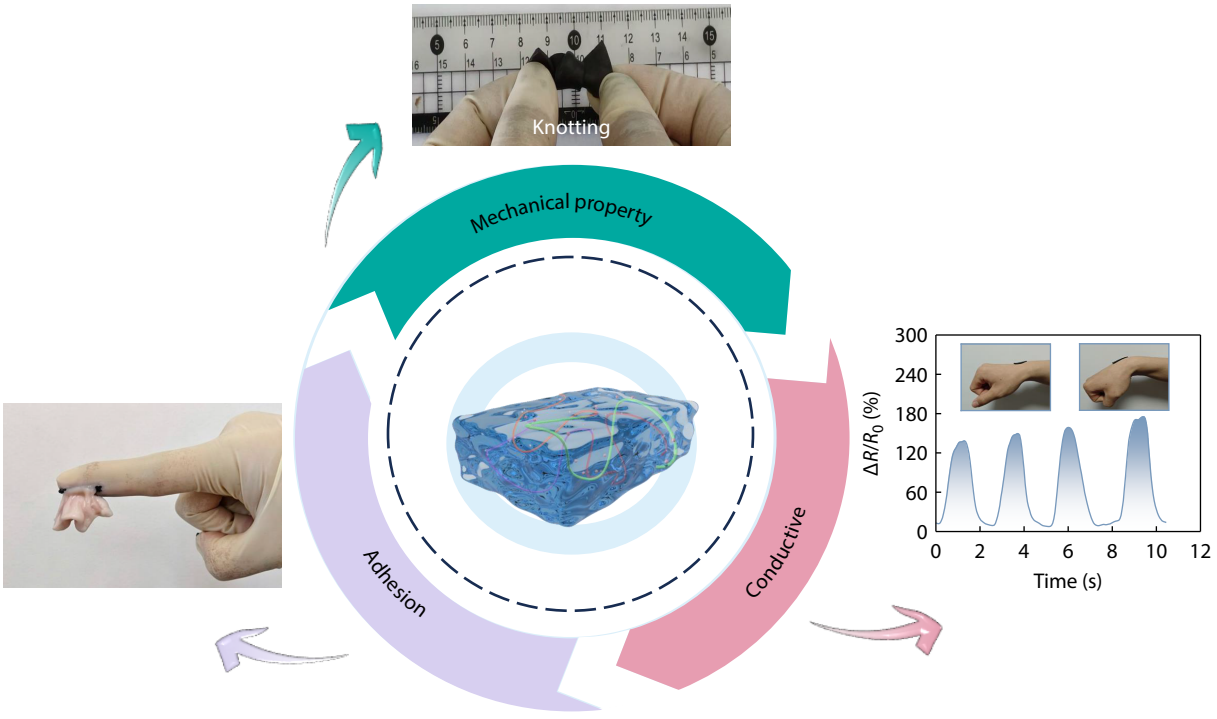

Chinese J. Polym. Sci., 2026 *https://doi.org/10.1007/s10118-026-3754-y*

6 Jiang, W.; Peng, Y.; Yao, J.; Li, Z.; Wang, L.; Liu, W. Cellulose and gum Arabic based nanocomposite hydrogel sensors for health monitoring and emergency medical signaling. *Int. J. Biol. Macromol.* **2025**, *323*, 147111.

7 Zhang, J.; He, Z.; Shen, B.; Li, J.; Tang, Y.; Pang, S.; Tian, X.; Wang, S.; Li, F. Mechanically tunable composite hydrogel for multi-gesture motion monitoring. *Biosensors* **2025**, *15*, 412.

8 Ju, H.; Jeong, J.; Kwak, P.; Kwon, M.; Lee, J. Robotic flexible electronics with self-bendable films. *Soft Robot.* **2018**, *5*, 710–717.

9 Dellatolas, I.; Bantawa, M.; Damerau, B.; Guo, M.; Divoux, T.; Del Gado, E.; Bischofberger, I. Local mechanism governs global reinforcement of nanofiller-hydrogel composites. *ACS Nano* **2023**, *17*, 20939–20948.

10 Qiu, A.; Jia, Q.; Yu, H.; Oh, J.-A.; Li, D.; Hsu, H.-Y.; Kawashima, N.; Zhuge, Y.; Ma, J. Highly sensitive and flexible capacitive elastomeric sensors for compressive strain measurements. *Mater. Today Commun.* **2021**, *26*, 102023.

11 Elangwe, C. N.; Morozkina, S. N.; Olekhnovich, R. O.; Krasichkov, A.; Polyakova, V. O.; Uspenskaya, M. V. A review on chitosan and cellulose hydrogels for wound dressings. *Polymers* **2022**, *14*, 5163.

12 Elnemr, M.; Halawani, Y.; Elkaffas, R. A.; Elkaffas, R.; Samad, Y. A.; Hisham, M.; Mohammad, B.; Butt, H. Artificial intelligence-enabled 4D printed hydrogel wearables: temperature and ultraviolet monitoring. *ES Mater. Manuf.* **2025**, *27*, 1428.

13 Hu, L.; Chee, P.-L.; Sugiarto, S.; Yu, Y.; Shi, C.; Yan, R.; Yao, Z.; Shi, X.; Zhi, J.; Kai, D.; Yu, H.-D.; Huang, W. Hydrogel-based flexible electronics. *Adv. Mater.* **2023**, *35*, 2205326.

14 Liang, Y.; Qiao, L.; Qiao, B.; Guo, B. Conductive hydrogels for tissue repair. *Chem. Sci.* **2023**, *14*, 3091–3116.

15 Mecwan, M.; Li, J.; Falcone, N.; Ermis, M.; Torres, E.; Morales, R.; Hassani, A.; Haghniaz, R.; Mandal, K.; Sharma, S.; Maity, S.; Zehtabi, F.; Zamanian, B.; Herculano, R.; Akbari, M.; John, J. V.; Khademhosseini, A. Recent advances in biopolymer-based hemostatic materials. *Regen. Biomater.* **2022**, *9*, rbac063.

16 Wang, Z.; Wei, H.; Huang, Y.; Wei, Y.; Chen, J. Naturally sourced hydrogels: Emerging fundamental materials for next-generation

healthcare sensing. *Chem. Soc. Rev.* **2023**, *52*, 2992–3034.
17 Yan, X.; Li, H.; Wang, T.; Li, A.; Zhu, C.; Lu, G. Engineering of coordination environment in bioinspired laccase-mimicking catalysts for monitoring of pesticide poisoning. *Chem. Eng. J.* **2022**, *446*, 136930.
18 Zhang, Z.; Fu, H.; Li, Z.; Huang, J.; Xu, Z.; Lai, Y.; Qian, X.; Zhang, S. Hydrogel materials for sustainable water resources harvesting & treatment: Synthesis, mechanism and applications. *Chem. Eng. J.* **2022**, *439*, 135756.
19 Chen, L.; Wang, W.; Lin, Z.; Lu, Y.; Chen, H.; Li, B.; Li, Z.; Xia, H.; Li, L.; Zhang, T. Conducting molybdenum sulfide/graphene oxide/polyvinyl alcohol nanocomposite hydrogel for repairing spinal cord injury. *J. Nanobiotechnol.* **2022**, *20*, 210.
20 Ho, M.; Ramirez, A. B.; Akbarnia, N.; Croiset, E.; Prince, E.; Fuller, G. G.; Kamkar, M. Direct ink writing of conductive hydrogels. *Adv. Funct. Mater.* **2025**, *35*, 2415507.
21 Wang, X.; Zheng, S.; Xiong, J.; Liu, Z.; Li, Q.; Li, W.; Yan, F. Stretch-induced conductivity enhancement in highly conductive and tough hydrogels. *Adv. Mater.* **2024**, *36*, 2313845.
22 Grosskopf, A. K.; Mann, J. L.; Baillet, J.; Lopez Hernandez, H.; Autzen, A. A. A.; Yu, A. C.; Appel, E. A. Extreme extensibility in physically cross-linked nanocomposite hydrogels leveraging dynamic polymer–nanoparticle interactions. *Macromolecules* **2022**, *55*, 7498–7511.
23 Zhou, T.; Wang, Y.; Zhou, J.; Yao, L.; He, K.; Chen, L.; Zhang, S.; Liu, H.; Chen, X.; Cui, S. Inorganic hydrogels can be flexible and highly extensible. *Adv. Mater.* **2025**, *37*, 2503910.
24 Zhang, X.; Zhang, H.; Lv, X.; Xie, T.; Chen, J.; Fang, D.; Yi, S. One-step of ionic liquid-assisted stabilization and dispersion: Exfoliated graphene and its applications in stimuli-responsive conductive hydrogels based on chitosan. *Int. J. Biol. Macromol.* **2024**, *271*, 132699.
25 Tropp, J.; Collins, C. P.; Xie, X.; Daso, R. E.; Mehta, A. S.; Patel, S. P.; Reddy, M. M.; Levin, S. E.; Sun, C.; Rivnay, J. Conducting polymer nanoparticles with intrinsic aqueous dispersibility for conductive hydrogels. *Adv. Mater.* **2024**, *36*, 2306691.
26 Huang, C.; Jiao, H.; Dang, R. Preparation of electroconductive hydrogel and its application in the sensing field. *Mater. Today Commun.* **2025**, *49*, 114319.
27 Yang, J.; Chen, Y.; Zhao, L.; Zhang, J.; Luo, H. Constructions and properties of physically cross-linked hydrogels based on natural polymers. *Polym. Rev.* **2023**, *63*, 574–612.
28 Klonos, P. A.; Bikiaris, R. D.; Terzopoulou, Z.; Mouchlianiti, K.; Tsachouridis, K.; Anastasiou, A. D.; Kyritsis, A.; Kyzas, G. Z. Structure-properties relationships in new polymer nanocomposites based on the renewable poly(butylene succinate) filled with low amounts of nanoparticles of 1-3D geometries. *Polymer* **2024**, *296*, 126841.
29 Mendhe, A. C.; Rengasamy, M.; Pradeep, H.; Bhoyar, T.; Chandirasekar, K.; Kore, A.; Elayappan, V.; Mendhe, A. B.; Mandal, S.; Rajaram, K.; Barse, N. S.; Hussain, I.; Kim, M.; Jadhav, S. B.; Noh, H. S.; Kim, Y.; Sun, M.; Lee, H. Recent advances and insights into carbon-based materials synergistically enhancing MXene for supercapacitor, battery, solar cell, and electrocatalytic applications. *Coord. Chem. Rev.* **2026**, *550*, 217400.
30 Chen, G.; Guo, Y.; Hsiao, S. B.; Hou, K.; Zhu, M. Tough, conductive hydrogels with double-network based on hydrophilic polymer assistant well-dispersed carbon nanotube for innovative force sensor. *Sci. China Technol. Sci.* **2022**, *65*, 1160–1168.
31 Kim, H.; Song, H.; Çakmakçı, N.; Kang, H.; Park, J.; Shin, M.; Jeong, Y. A flexible supercapacitor prepared with surface modified carbon nanotube film electrode and hydrogel electrolyte. *Fibres. Polym.* **2021**, *22*, 2673–2679.
32 Kumar, R.; Cho, Y. S.; Kim, S. M. Carbon nanotubes for high-performance energy storage devices. *Carbon Lett.* **2026**, *36*, 1–20.
33 Li, Z.; Tang, M.; Bai, W.; Bai, R. Preparation of hydrophilic encapsulated carbon nanotubes with polymer brushes and its application in composite hydrogels. Langmuir **2017**, *33*, 6092–6101.
34 Khan, M.; Ali Shah, L.; Rahman, T. U.; Ara, L.; Yoo, H.-M. Multiple-language-responsive conductive hydrogel composites for flexible strain and epidermis sensors. *ACS Appl. Polym. Mater.* **2024**, *6*, 4233–4243.
35 Kamaliya, B.; Dave, P. N.; Macwan, P. M. Oxidized multiwalled carbon nanotube reinforced rheological examination on Gum ghatti-*cl*-*poly*(acrylic acid) hydrogels. *J. Appl. Polym. Sci.* **2022**, *139*, e52888.
36 Fu, C.; Zhou, M.; Fu, H. Agarose-sodium alginate hydrogel beads enhanced with zeolitic imidazolate frameworks/multiwalled carbon nanotubes nanoparticles for efficient adsorption and selective separation of methylene blue. *J. Appl. Polym. Sci.* **2024**, *141*, e55003.
37 Wang, Y.; Li, L.; Ma, Y.; Tang, Y.; Zhao, Y.; Li, Z.; Pu, W.; Huang, B.; Wen, X.; Cao, X.; Chen, J.; Chen, W.; Zhou, Y.; Zhang, J. Multifunctional supramolecular hydrogel for prevention of epidural adhesion after laminectomy. *ACS Nano* **2020**, *14*, 8202–8219.
38 Khademi, Z.; Nikoofar, K. Applications of catalytic systems containing DNA nucleobases (adenine, cytosine, guanine, and thymine) in organic reactions. *RSC Adv.* **2025**, *15*, 3192–3218.
39 Shi, Y.; Li, D.; Ding, J.; He, C.; Chen, X. Physiologically relevant pH- and temperature-responsive polypeptide hydrogels with adhesive properties. *Polym. Chem.* **2021**, *12*, 2832–2839.